

# Phase Separation in a Polymer Solution Induced by Steady and Large Amplitude Oscillatory Shear Flow

S. Saito,<sup>†</sup> T. Hashimoto,<sup>†</sup> I. Morfin,<sup>‡</sup> P. Lindner,<sup>‡</sup> F. Boué,<sup>§</sup> and D. J. Pine<sup>\*,‡</sup>

Department of Polymer Chemistry, Graduate School of Engineering, Kyoto University, Kyoto 606-8501, Japan, Institut Laue-Langevin, BP 156, F.-38042, Grenoble Cedex 9, France, Laboratoire Léon Brillouin, CEN Saclay, F-91191 Gif sur Yvette, France, and Departments of Chemical Engineering and Materials, University of California, Santa Barbara, California 93106-5080

Received June 3, 2002

**ABSTRACT:** Neutron- and light-scattering measurements reveal that large-amplitude oscillatory shear flow can drive entangled polymer solutions to a completely microphase-separated state with sharp interfacial boundaries while steady shear flow does not. For steady shear flow, interfacial boundaries remain less well-defined for all shear rates measured, indicating less complete phase separation. Results are discussed within the context of recent theoretical models.

## I. Introduction

Entangled polymer solutions are much more sensitive to shear flow than are conventional liquids. This extreme sensitivity is closely related to the very slow system dynamics that result from the entanglement of long polymer molecules. From a practical point of view, this sensitivity has important consequences for polymer processing, since the microstructure of the polymer solution can be altered significantly by stirring or molding. From a more fundamental point of view, these systems provide fertile ground for exploring the coupling of flow to fluid microstructure and for studying the statistical mechanics of systems driven far from equilibrium.

The effects of shear flow on entangled polymer solutions are particularly strong in the vicinity of the demixing phase transition.<sup>1</sup> The application of a modest shear flow can cause a transparent polymer solution to become cloudy to the point of being completely opaque. Such observations have led to speculation that shear flow drives such a system to phase separate, at least on some microscopic length scale which is nevertheless sufficiently large to strongly scatter light.<sup>2</sup> Despite many experimental investigations, however, direct evidence for a shear-induced phase separation has been lacking.

We present light- and neutron-scattering experiments which provide strong evidence that shear flow can cause a complete demixing phase transition in an entangled polymer solution. The most interesting result is that large amplitude *oscillatory* shear flow can cause the system to phase separate into small domains with *sharp interfacial boundaries*. By contrast, the interfacial boundaries which develop under steady shear flow are less well-defined, indicating that the demixing phase transition is less complete. The observation that oscillatory shear flow is more effective than steady shear flow in promoting complete phase separation is surprising and not anticipated by theory.<sup>3–5</sup> Nevertheless, by extending concepts introduced in recent models,<sup>3–5</sup> we

propose a mechanism for these new results which is consistent with our measurements.

## II. Experiments

For this study, we prepared a solution of deuterated polystyrene (dPS) in dioctyl phthalate using established procedures.<sup>6</sup> The weight-average molecular weight  $M_w$  of the dPS was  $2.00 \times 10^6$ ; the concentration  $c$  was 8 wt %. This corresponds to a semidilute solution with  $dc^* = 6.4$ , where  $c^*$  is the overlap concentration. We note that DOP is a  $\Theta$  solvent for dPS at a temperature of 7 °C. Although the cloud point of this solution has not been determined, the solution was clearly in a single phase at  $T = 9$  °C. All experiments were carried out at higher temperatures, ensuring that the equilibrium system was a single phase.

Measurements of small-angle light scattering (SALS) were performed under both steady and oscillatory shear flow using a transparent cone-plate shear cell made of quartz. It had a diameter of 80 mm and a cone angle of 1.0°. A detailed description of the apparatus can be found in ref 7. We use a Cartesian coordinate system with the  $x$  axis parallel to the flow direction, the  $y$  axis parallel to the shear gradient direction, and the  $z$  axis parallel to the vorticity direction. The incident laser has a wavelength of 632.8 nm and propagates along the  $y$  direction, giving a two-dimensional small-angle scattering pattern in the  $q_x$ - $q_z$  plane, where  $q_x$  and  $q_z$  are the scattering wavevectors along the  $x$  and  $z$  directions, respectively. The time dependent strain in the oscillatory shear flow measurements is given by  $\gamma(t) = \gamma_0 \sin \phi(t)$  where  $\phi(t) = \omega t$ ,  $\gamma_0$  is the strain amplitude, and  $\omega$  is the angular frequency. Data for the SALS experiments under the oscillatory shear flow were collected at different fixed values of the strain phase  $\phi$  using a procedure described in ref 7.

Small-angle neutron scattering (SANS) was also performed under both steady and oscillatory shear flow. The experiments under steady shear flow were conducted at the D11 instrument of the Institut Laue-Langevin (ILL), Grenoble, France. A quartz Couette cell<sup>8</sup> was used to impose the steady shear flow. The incident neutron beam passed through the sample along the  $y$  direction, which enabled observation of the SANS in the same plane ( $q_x$ - $q_z$ ) as the SALS experiment. The experiments under oscillatory shear flow were carried out using the instrument SANS-J at the Japan Atomic Energy Research Institute (JAERI), Tokai, Japan. A sandwich-type shear cell<sup>6</sup> made of copper was used to impose an oscillatory shear flow. The incident neutron beam passed through the sample along the  $y$  direction, allowing us to observe SANS in the  $q_x$ - $q_z$  plane. The  $\phi$ -resolved data acquisition was conducted using the dynamic data acquisition system described in ref 9.

\* Corresponding author.

<sup>†</sup> Kyoto University.

<sup>‡</sup> Institut Laue-Langevin.

<sup>§</sup> CEN Saclay.

<sup>‡</sup> University of California, Santa Barbara.

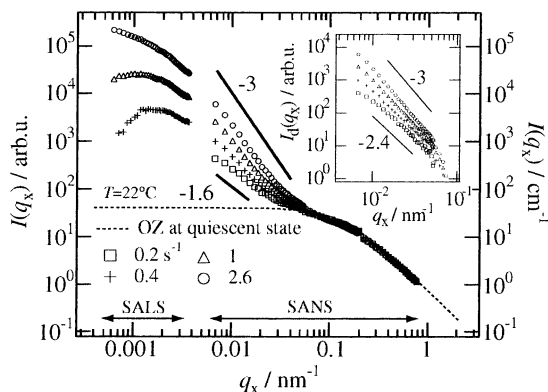


**Figure 1.** Steady-state scattering profiles  $I(q_x)$  parallel to the flow direction obtained under steady shear flow at four different shear rates and at 22 °C. The SALS intensity profiles (arbitrary units) were all multiplied by a single shift factor in order to smoothly connect with SANS profiles. The dotted line is the OZ function obtained by fitting the data for the quiescent state. The inset shows  $I_d(q_x)$  evaluated by subtracting the OZ contribution from the net scattering profiles  $I_d(q_x)$ .

**Small-Angle Neutron and Light Scattering.** We first imposed steady shear flow to the sample solution at 22 °C and obtained two-dimensional scattering patterns  $I(q_x, q_z)$  in the steady state for several different shear rates  $\dot{\gamma}$ . From these data, we extract the scattering intensity profiles along the flow direction  $I(q_x)$  and plot them as a function of  $q_x$  in Figure 1. The magnitude of the scattering wavevector is given by  $q = |\mathbf{q}| = (4\pi/\lambda) \sin(\theta/2)$ , where  $\lambda$  and  $\theta$  are the wavelength and scattering angle in the medium, respectively. At  $\dot{\gamma} = 0.1 \text{ s}^{-1}$ , no excess scattering above the quiescent state was observed in either SALS or SANS in the  $q_x$ - $q_z$  plane (data not shown in the figure). At  $\dot{\gamma} = 0.2 \text{ s}^{-1}$ , the “butterfly pattern”,<sup>10</sup> characteristic of shear-induced structure formation, was observed using SANS, which covers a range of wavevectors  $6.76 \times 10^{-3} < q < 7.8 \times 10^{-1} \text{ nm}^{-1}$ . At the same shear rate, no excess scattering was observed in the SALS pattern, which covers a range of wavevectors  $6.2 \times 10^{-4} < q < 3.7 \times 10^{-3} \text{ nm}^{-1}$ . For  $0.4 \leq \dot{\gamma} \leq 2.6 \text{ s}^{-1}$ , the butterfly patterns appeared in both SALS and SANS.

The equilibrium scattering is described very well by the Ornstein–Zernike (OZ) equation  $I(q) = I(0)/(1 + q^2\xi^2)$  with an equilibrium correlation length of  $\xi \approx 7.6 \text{ nm}$ . Note that the excess scattering caused by shear is observed only for wavevectors below the shoulder in the equilibrium scattering pattern. Thus, excess scattering occurs only on length scales larger than the equilibrium correlation length  $\xi$ , consistent with recent theories of shear-enhanced concentration fluctuations in entangled polymer solutions.<sup>3–5</sup> Physically, this means that shear introduces new correlated structures on length scales larger than  $\xi$ ; at length scales smaller than  $\xi$ , the equilibrium fluctuations persist unmodified from the equilibrium state. The SANS profiles for  $q \lesssim 0.06 \text{ nm}^{-1}$  show power law behavior  $I(q_x) \sim q_x^{-a}$  with exponents  $a$  between 1.6 and 3.

**Decomposition of Scattering Results.** The scattering profile of the sheared system can be decomposed into two functions:<sup>6</sup> the OZ scattering function  $I_{\text{OZ}}(q_x)$  representing the equilibrium fluctuations, and a scattering function  $I_d(q_x)$  reflecting the excess scattering due to shear. Such a decomposition is useful for isolating the different contributions to the scattering and is justified at the end of the Discussion.

To extract  $I_d(q_x)$ ,  $I_{\text{OZ}}(q_x)$  was first evaluated by the fitting the SANS profile with the OZ function for  $q \gtrsim 0.06 \text{ nm}^{-1}$ . Then  $I_{\text{OZ}}(q_x)$  was subtracted from the full scattering function  $I(q_x)$ . The intensity profiles  $I_d(q_x)$  thus obtained are shown in the inset to Figure 1. The SALS data were not significantly affected by this operation, and are not included in the inset. The power law behavior  $I_d(q_x) \sim q_x^{-a}$  is still observed with  $a$  between 2.4 and 3.

To explore the temperature dependence of the excess scattering due to shear, the temperature was decreased to 12.2

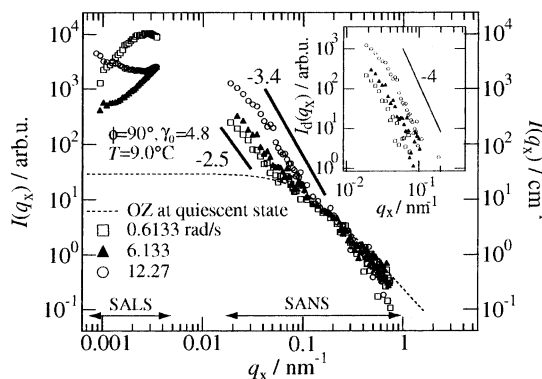


**Figure 2.** Steady-state scattering profiles parallel to the flow direction obtained under oscillatory shear flow. The SALS intensity profiles were all multiplied by a single shift factor in order to smoothly connect with SANS profiles. The dotted line is the OZ function obtained by fitting the data for the quiescent state. The inset shows  $I_d(q_x)$  evaluated by subtracting the OZ contribution from the scattering profiles.

°C while keeping  $\dot{\gamma} = 2.6 \text{ s}^{-1}$ . In this experiment, we found that  $I_d(q_x) \sim q_x^{-a}$  with  $a = 3$  independent of temperature.<sup>11</sup> Thus, the exponent  $a$  does not become larger than 3 for steady shear flow over the range of temperatures and shear rates covered in these experiments. It is significant that  $a$  remains less than 4, the value expected from the Porod law for scattering from two-phase structures with well-defined sharp interfaces. This indicates that *steady* shear flow does not induce well-defined two-phase structures with sharp interfaces. We next turn our attention to the experiments performed under oscillatory shear flow at an angular frequency  $\omega$  and strain amplitude  $\gamma_0$ . As previously reported,<sup>12</sup> the scattering intensity observed under large amplitude oscillatory shear flow develops and decays synchronously with  $\phi$ . Hence, we focus on data obtained at  $\phi = 90^\circ$ , where the strain and scattering amplitudes reach their maximum values. All measurements were carried out with a strain amplitude  $\gamma_0 = 4.8$  and at a temperature  $T = 9.0 \text{ °C}$ . Two-dimensional excess scattering patterns were observed in both SALS and SANS for  $0.6133 \leq \omega \leq 12.27 \text{ rad/s}$ . As  $\omega$  increased, the butterfly pattern in the SANS  $q$ -region became sharper and more intense, while the SALS pattern lost its characteristic two lobes and became almost isotropic. This means that the characteristic length scale of the shear-induced structures becomes smaller with increasing  $\omega$ . Figure 2 shows the scattering profiles in the  $q_x$ -direction. The excess scattering from the structures induced by the oscillatory shear can be seen in the  $q$ -region less than about  $0.1 \text{ nm}^{-1}$ . At  $\omega = 0.6133 \text{ rad/s}$ , a scattering peak is observed in the SALS  $q$ -region. Although a scattering peak at  $\omega = 6.133 \text{ rad/s}$  cannot be observed within our experimental  $q$ -window, we can deduce its existence and can trace the peak positions  $q_{\text{m}}$  from the shape of the SALS and SANS profiles. From these data, it is clear that  $q_{\text{m}}$  moves toward higher  $q$  with increasing  $\omega$ , indicating the shear-induced structures become smaller with increasing  $\omega$ . When  $\omega$  is increased to 12.27 rad/s, the scattering increases at small  $q$  indicating that, in addition to the aforementioned small structures, some larger scale structures also appear. While outside the scope of the present investigation, this may indicate incipient macroscopic phase separation. Further experiments are necessary to investigate this possibility.

To extract the excess scattering  $I_d(q_x)$  due to shear, we used the same procedure previously employed for steady shear flow. The results are shown in the inset to Figure 2. Prior to the subtraction of  $I_{\text{OZ}}(q_x)$ , the raw data exhibit power law behavior in the SANS  $q$ -region between 0.02 and  $0.1 \text{ nm}^{-1}$ , with  $a$  increasing from 2.5 to 3.4 with increasing  $\omega$ . After correcting for the OZ contribution, however, the data exhibit a power law with  $a \approx 4$  for all values of  $\omega$ , indicating that the oscillatory shear flow causes the system to develop phase-separated domains with well-defined interfaces. In contrast, for steady shear flow, we obtain a power law with  $a \approx 3$ . Thus, a

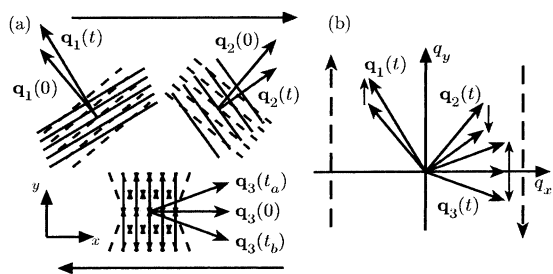


**Figure 3.** (a) Distortion by shear flow of fluctuations in real space. (b) Trajectories in  $q$ -space of fluctuations distorted by shear flow. Fluctuations are rotated clockwise by a steady shear flow, as illustrated by  $\mathbf{q}_1(t)$  and  $\mathbf{q}_2(t)$ , while oscillatory shear flow rotates fluctuations back and forth, as illustrated by  $\mathbf{q}_3(t)$ .

comparison of these data sets indicates that oscillatory shear flow drives the system to a completely microphase-separated state with domains having sharply defined interfaces while steady shear flow does not.

### III. Discussion

To our knowledge, none of the currently available theories describe our data. However, the theory first proposed by Helfand and Fredrickson,<sup>3</sup> and later extended by Milner<sup>4</sup> and Onuki<sup>5</sup> (hereafter referred to as HFMO), can provide a framework for developing qualitative insight into our results. According to the HFMO theory, spontaneous fluctuations of the polymer concentration can be enhanced by shear flow, depending upon their size and orientation with respect to the flow. To see how this works, we recall that the scattering intensity  $I(\mathbf{q})$  measured in experiments is, aside from numerical constants, equal to  $\langle \delta c(\mathbf{q}) \delta c(-\mathbf{q}) \rangle$ , where  $\delta c(\mathbf{q})$  is the spatial Fourier transform of the concentration fluctuations  $\delta c(\mathbf{r})$  and the brackets  $\langle \dots \rangle$  indicate an ensemble (or time) average. Physically,  $\delta c(\mathbf{q}, t)$  represents a sinusoidal concentration fluctuation of wavelength  $2\pi/q$  with planes of constant concentration oriented perpendicular to  $\mathbf{q}$ . In the simplest version of the HFMO theory, the *shear* stress associated with an externally applied shear flow *enhances* fluctuations  $\delta c(\mathbf{q}, t)$  which are oriented such that  $q_x = q_y$  and *diminishes* fluctuations which are oriented such that  $q_x = -q_y$ , as discussed below. The *normal* stresses most strongly enhance fluctuations when  $\mathbf{q}$  is oriented along the flow direction  $x$ . This is why the butterfly patterns in the  $q_x$ - $q_y$  plane are most intense along the  $q_x$  direction. This simple picture is complicated somewhat by the fact that the imposed shear flow changes the orientation and wavelength of the concentration fluctuations with time. The effect of shear flow on different Fourier components of the concentration fluctuations  $\delta c(\mathbf{q})$  is illustrated in Figure 3. It is clear from the figure that one effect of the shear flow  $v_x = \dot{\gamma}y$  is to rotate the fluctuations clockwise; shear flow also stretches or compresses the wavelength of the fluctuations depending upon their orientation. A careful examination of the effect of such a shear flow reveals that the trajectory of a concentration fluctuation with wavevector  $\mathbf{q}(0)$  at some arbitrary reference time  $t = 0$  is given by<sup>3</sup>

$$\mathbf{q}(t) = q_x(0)\hat{\mathbf{e}}_x + [q_y(0) - q_x(0)\gamma(t)]\hat{\mathbf{e}}_y + q_z(0)\hat{\mathbf{e}}_z \quad (1)$$

where for steady shear flow the strain  $\gamma(t)$  is given by  $\dot{\gamma}t$  with  $\dot{\gamma} = \text{constant}$ . This corresponds to the wavevector of a fluctuation being convected in the  $-q_y$  direction if

$q_x > 0$  and along the  $+q_y$  direction if  $q_x < 0$  (see Figure 3). An examination of eq 1 and Figure 3 reveals that this convection drives all fluctuations toward the second ( $x < 0, y > 0$ ) or fourth ( $x > 0, y < 0$ ) quadrants of the  $q_x$ - $q_y$  plane (except those for which  $q_x = 0$ ) and then toward *large*  $q$ . Thus, fluctuations which happen to be oriented such that they are in regions of high growth (the first and third quadrants) cannot grow indefinitely since they will ultimately be convected away from the regions of high growth and into the regions of high dissipation (and high  $q$ ) in the second and fourth quadrants. There they will be destroyed by diffusion (at a rate of  $Dq^2$ ). As pointed out by Helfand and Fredrickson,<sup>3</sup> this acts as a stabilizing mechanism which limits the growth of concentration fluctuations.

Next we consider what happens to fluctuations under *oscillatory* shear flow. In this case, the total strain  $\gamma(t)$  appearing in eq 1 is  $\gamma(t) = \gamma_0 \sin \omega t$  where the strain amplitude  $\gamma_0$  is a constant. Thus, for a system subjected to oscillatory shear flow, the trajectory of any fluctuation in  $q$ -space will also oscillate. Since the oscillating strain  $\gamma(t)$  cannot grow larger than the amplitude  $\gamma_0$ , this will confine a fluctuation to a given region of  $q$ -space, as illustrated in Figure 3.

First we consider the enhancement of fluctuations by oscillating normal stresses. Under oscillatory shear flow, a fluctuation which is initially oriented near the  $q_x$  axis will oscillate about the  $q_x$  axis and thus will repeatedly pass near the  $q_x$  axis where the enhancement of fluctuations by normal stresses is strongest. Thus, the convective stabilizing mechanism that limits the amount of time that fluctuations can spend in the high growth region of  $q$ -space is absent. Lacking this stabilizing mechanism, the oscillating shear flow can drive the system all the way to a completely phase-separated state characterized by sharp interfacial boundaries. This is consistent with what is observed experimentally.

Now we consider the enhancement of fluctuations by shear stresses. The argument here is complicated by the fact that the *regions* in  $q$ -space of high growth do not remain in a fixed region of  $q$ -space but *oscillate* in time with the shear flow. That is, for an oscillating shear rate given by  $\dot{\gamma} = \gamma_0 \omega \cos \omega t$ , the regions of enhanced growth are around  $q_x = q_y$  when  $\cos \omega t > 0$  and are around  $q_x = -q_y$  when  $\cos \omega t < 0$ . Conversely, the regions of enhanced dissipation are around  $q_x = -q_y$  when  $\cos \omega t > 0$  and are around  $q_x = q_y$  when  $\cos \omega t < 0$ . Thus, fluctuations are subjected to shear forces which alternately enhance and then diminish their growth. Thus, fluctuations should not be enhanced as much by shear stresses under oscillatory flow as under steady flow. According to HFMO theory, the small  $q$  region is where the effect of *shear* stresses on concentration fluctuations is strongest.<sup>4</sup> Thus, at small  $q$ , we expect the fluctuations under oscillatory flow to be suppressed relative to steady shear flow (but not relative to no flow). Referring to Figures 1 and 2, we see that this is exactly what is observed. We speculate that the movement of the peak in Figure 2 is caused primarily by the growing influence of normal stresses as the strain frequency (and hence characteristic shear rate) is increased.

We return now to the justification for subtracting out the equilibrium Ornstein-Zernicke scattering from the total scattering. First, we note that we are concerned only with fluctuations in the  $\hat{\mathbf{e}}_x$  direction (see Figures 1 and 2). As can be seen from eq 1, fluctuations that are spontaneously born at a wavevector  $\mathbf{q} = (q_x, 0, 0)$  are

convected away by the shear flow (in the  $\pm \hat{e}_y$  direction) to different wavevectors where they ultimately dissipate. At the same time, *new* thermal fluctuations are constantly being created at all wavevectors, specifically those near  $\mathbf{q} = (q_x, 0, 0)$ . Thus, at a wavevector  $\mathbf{q} = (q_x, 0, 0)$  along the  $q_x$  axis, there are, crudely speaking, two kinds of fluctuations, newly created fluctuations on which the shear flow has had little time to act and fluctuations created some time earlier (generally, at some other wavevector) on which the shear flow and its associated stresses has had significant time to act. By subtracting out the equilibrium Ornstein–Zernicke scattering, we are able to isolate those fluctuations that the shear flow has significantly distorted from equilibrium. While such a subtraction scheme is crude and rigorously speaking too simplistic, such an analysis does serve the useful purpose of illustrating how large amplitude shear flow leads to a steady state that is characterized by much more sharply defined interfaces than does steady shear flow. It also demonstrates the role of *steady* shear flow in transporting fluctuations from one region of  $q$ -space where fluctuations grow to another where fluctuations are suppressed and dissipated. In oscillatory shear flow, fluctuations are allowed to grow longer so that sharper interfaces can develop.

#### IV. Conclusions

The nonequilibrium situation created by imposing a shear flow on a polymer solution is fundamentally different from that which exists under many other nonequilibrium situations. In spinodal decomposition, for example, no steady state ever develops; there is only a steady progression from equilibrium toward phase separation by a progressive coarsening of the concentration fluctuations of the polymer. In a shear flow, by contrast, new equilibrium fluctuations are constantly being created, grown, stretched, and ultimately dissipated. The same shear flow that causes equilibrium fluctuations to grow also limits their ultimate growth. The experimental results presented here demonstrate that phase separation can proceed much farther, toward more sharply defined interfaces, by using an oscillatory

shear flow, which confines fluctuations to a region of  $q$ -space where the shear-induced growth is strongest.

We have argued that the data presented here can be rationalized in terms of the existing theoretical framework provided by HFMO. Nevertheless, our explanations are qualitative in nature and do not yet represent a full quantitative explanation of the data. As such, these experimental results pose a new challenge for our understanding of the effects of shear flow on the internal structure of polymeric liquids. The effects we observe are strongly nonlinear, being observed only at rather large strain amplitudes ( $\gamma_0 = 4.8$  in these measurements) and in a region where normal stresses are dominant. At a minimum, solutions to the currently existing HFMO model must go beyond the linear approximations that are currently available.

**Acknowledgment.** T.H. acknowledges a Grant-in-Aid for Scientific Research (under Grant No. 12305060A) from Japan Society for the Promotion of Science for financial support. D.P. thanks the John Simon Guggenheim Memorial Foundation and the National Science Foundation (Award No. DMR-9870128) for financial support.

#### References and Notes

- (1) Larson, R. G. *Rheol. Acta* **1992**, *31*, 497–520.
- (2) Rangel-Nagel, C.; Metzner, A.; Wissbrun, C. *Macromolecules* **1984**, *17*, 1187.
- (3) Helfand, E.; Fredrickson, G. H. *Phys. Rev. Lett.* **1989**, *62*, 2468–2471.
- (4) Milner, S. T. *Phys. Rev. E* **1993**, *48*, 3674–3691.
- (5) Onuki, A. *J. Phys.: Condens. Matter* **1997**, *9*, 6119–6157.
- (6) Saito, S.; Koizumi, S.; Matsuzaka, K.; Suehiro, S.; Hashimoto, T. *Macromol.* **2000**, *33*, 2153–2162.
- (7) Matsuzaka, K.; Hashimoto, T. *Rev. Sci. Instrum.* **1999**, *70*, 2387–2397.
- (8) Lindner, P.; Oberthur, R. *Colloid Polym. Sci.* **1985**, *263*, 443.
- (9) Koizumi, S.; Saito, S.; Suehiro, S.; Hashimoto, T. Unpublished work.
- (10) Hashimoto, T.; Fujioka, K. *J. Phys. Soc. Jpn.* **1991**, *60*, 356–359.
- (11) Saito, S.; Hashimoto, T.; Morfin, I.; Lindner, P.; Boue, F. *Macromolecules* **2002**, *35*, 445–459.
- (12) Saito, S.; Matsuzaka, K.; Hashimoto, T. *Macromolecules* **1999**, *32*, 4879–4888.

MA0208584